Coordinating Energy Resources in an Islanded Microgrid for Economic and Resilient Operation

Linli Jia, *Student Member, IEEE*, Sanjeev Pannala, *Member, IEEE*, Gowtham Kandaperumal, *Member, IEEE*, and Anurag Srivastava, *Fellow, IEEE*

***Abstract*—Microgrids with advanced management and control strengthen power system reliability and resilience. In normal operation, economy and reliability are the objectives. However, for adverse events, economy would not be the top concern and focus moves to resiliency and providing energy to critical loads. The resource dispatch strategy in normal economic mode would not be suitable for resilient mode given adverse events. In this work, an energy resource coordination strategy is proposed for a hydro–diesel-battery islanded microgrid, which improves distribution system resiliency by preevent control and switching to resilient mode from economic mode. Resiliency metric is used to verify and quantify the effectiveness of the selected strategy among available ones. Real-time resiliency management system (RT-RMS), a real time resilience management and visualization tool is developed and the resiliency driven resource coordination is integrated into it. Finally, a 14-nodes isolated power system model and a simplified 55-nodes real-world islanded microgrid model are used for validation and demonstrate the effectiveness of proposed resource coordination method.**

***Index Terms*—Economic versus resilient mode, energy storage, high impact low frequency (HILF) event, islanded microgrid, resource coordination and dispatch, resilience metric.**

I. Introduction

LAST decades have witnessed a significant increase of power system failures caused by extreme weather events, which are usually characterized as high impact low frequency (HILF) events. Traditionally, power system performance is evaluated by reliability metrics. However, they are not suitable for evaluating power grid's ability to face the HILF events, because reliability estimation is based on historical data under normal and expected minor contingencies scenario, and does not capture HILF events. HILF events are usually more extreme and devastating, such as hurricanes, earthquakes, avalanches [1]. These events generally lead to large-scale destruction and impact to power systems, which can last for a long time [1]. Under this background, the concept of power system resiliency is proposed. The concept of resiliency was first defined for the ecological system in 1973 [2], and since then resiliency of various disciplines and systems have been researched. Generally, resiliency refers to the ability of a system to predict, withstand large external disturbances, and to recover to normal operation state [3].

Also, power system resiliency quantification has attracted many researcher's interests. It is recognized that four aspects should be considered in power grid resilience evaluation [4]: "the capability to withstand event strike, the speed of recovery, planning capacity, and the capability to adapt event scenarios." Resilience measurement index of power system was first proposed by Argonne National Laboratory in 2013 as "the ability of an entity to anticipate, resist, absorb, respond to, adapt to, and recover from a disturbance," which is categorized into four phases: preparedness, mitigation, response, and recovery [5]. A framework for creating resilience metrics named resilience analysis process (RAP) [6] was proposed in 2015 and extended later [7], which specify criteria that resilience metrics should meet and the developing steps to follow. This enables users to customize resilience metrics for a specific analysis purpose. Carrington *et al.* [8] provided a general way to extract resilience metrics from utility data by decomposing resilience curve into an outage process and a restore process, and derive formulas for resilience metrics calculation. Resilience quantification framework built around the concept of "resiliency trapezoid" is proposed [3], [9], [10], which quantify the recovery agility and identify the optimal resiliency enhancement strategies. A comparison between reliability and resilience metrics is shown in Table I [11], [12], where the time scale refers to the total time usually taken for power system to withstand and recover from the events that counted by reliability and resiliency metrics, respectively.

Microgrids are expected to strengthen power system reliability and resiliency significantly, and their deployments got rapidly increased all around the world in recent years [13], [14]. Microgrid is designed as a small group of distributed energy resources and loads, which could be operated in both grid-connected and standalone modes. There also exists islanded

Manuscript received July 31, 2021; revised November 4, 2021 and January 5, 2022; accepted February 12, 2022. Date of publication March 1, 2022; date of current version May 20, 2022. Paper 2021-ESC-0891.R2, presented at the 2021 IEEE Industry Applications Society Annual Meeting (IAS), Vancouver, BC Canada, Jun. 12–16, and approved for publication in the IEEE TRANSACTIONS ON INDUSTRY APPLICATIONS by the Energy Systems Committee of the IEEE Industry Applications Society. This work was supported by the US Department of Energy RADIANCE project and DEIA0000025 UI-ASSIST project. *(Corresponding author: Linli Jia.)*

Linli Jia and Sanjeev Pannala are with the Washington State University, Pullman, WA 99164 USA (e-mail: linli.jia@wsu.edu; sanjeev.pannala@wsu.edu).

Gowtham Kandaperumal was with the Washington State University, Pullman, WA 99164 USA, and now working with the ComEd, Chicago, IL 60680-5379 USA (e-mail: g.kandaperumal@wsu.edu).

Anurag Srivastava is with the Washington State University, Pullman, WA 99164 USA, and also with the West Virginia University, Morgantown, WV USA (e-mail: anurag.srivastava@mail.wvu.edu).

Color versions of one or more figures in this article are available at https://doi.org/10.1109/TIA.2022.3154337.

Digital Object Identifier 10.1109/TIA.2022.3154337

TABLE I
DIFFERENCES BETWEEN RELIABILITY AND RESILIENCY EVALUATION

Parameter	Reliability	Resiliency
Event impact	Low impact, high frequency events. Measured in frequency, duration of outage	High impact, low frequency events. Measured in power system response to unfavorable events
Event type	Event agnostic. Mainly quantify reliable operation of the grid and the service to its end customers.	More specific to the type of threat Depends on threat study to be researched and resilient against
Loads considered	All connected loads are counted	Mostly focus on critical loads
Event study duration	Short duration outages (generally less than five minutes) are not counted	All power loss needs to be counted
Time scale	Seconds ∼hours	Up to days
Metric	LOLP, SAIDI, SAIFI, MAIFI, CAIFI, CELID, CEMI, CEMM	Not standardized. Metrics based on general power system attributes, performance, resiliency features.

microgrids that only operate at standalone mode, usually for remote areas or islands that are separated from the mass power grid geographically. Usually various DERs and battery energy storage systems (BESS) are involved in microgrids, such as wind turbines (WT), photovoltaic (PV) panels, small hydro plants (SHPs). A lot of research has been done on the sizing of various resource components of microgrids [15]–[18], and resource configuration [19].

Operation of islanded microgrids could be challenging, especially under HILF events. A great deal of research is done on the operation and control strategies for islanded microgrids. Multiple frequency regulation strategies for microgrids are proposed in [20]–[22]. An energy dispatch strategy for an islanded microgrid intending to alleviate power fluctuation is proposed in [23] and [24]. Various objectives of control optimization for islanded microgrids have been explored, such as to compensate the variation of renewable energies and load, to shift peak load, and to reduce the curtailment of renewable energies, etc. [25]. Generally economy is the most concern in normal operation. Optimal power flow (OPF) is widely used in setting operating points for available generation resources, battery charging/discharging rate of islanded microgrids, with minimum cost as objective [26]–[31]. However, when a HILF event happens, the above power management objective is not the most concern anymore. It is preferable to maximize energy storage in advance so as to minimize the impacts that HILF events could bring about. So other than an economic-oriented power management strategy, a new resiliency-oriented strategy is needed in advance of HILF events.

In this work, a coordination strategy for hydro–diesel-battery in an islanded microgrid is proposed, proactively coping with expected HILF events. To our knowledge, this is one of the first works to propose proactively switching from economic mode to resilient mode for resource management under expected HILF events. This work is extended from our preliminary work in [32]. Key contributions of this work include the following:

1) Developed a resilience-based dispatch strategy for an islanded hydro–diesel-battery microgrid. Early event warning signal has been used, which makes sure energy storage system could be fully prepared before events strike. Flow chart of the proposed strategy is shown in Fig. 1. Specifically, the islanded microgrid operates under economic mode during normal condition and switch to resiliency mode in anticipation of HILF events.

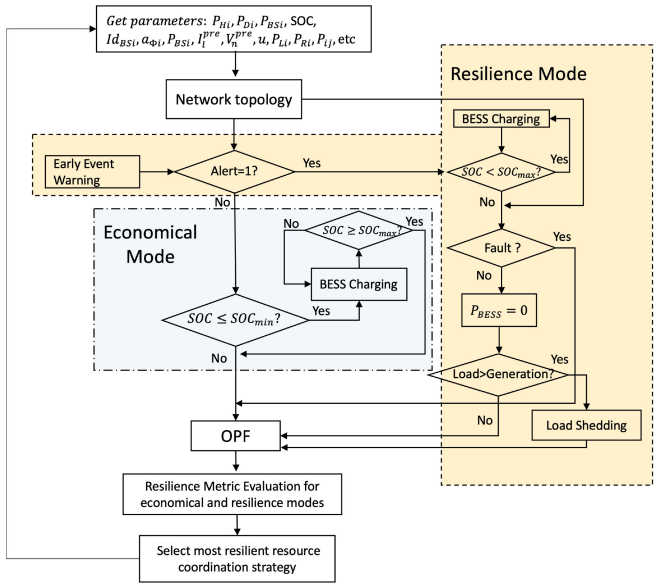

Fig. 1. Flow chart of the hydro–diesel-battery coordination strategy.

2) A set of resilience metrics is adopted to quantify and verify the resiliency improvements of the proposed strategy.
3) Integrated the developed strategy and use case within the real-time resiliency management system (RT-RMS) tool in development, enabling visualization of system resilience, and assisting operators in decision making.

II. RESILIENCY QUANTIFICATION

Generally, resilience metrics can be categorized into two groups: attribute-based and performance-based. Attribute-based metrics evaluate options enhancing grid resilience, such as robustness, resourcefulness, adaptivity, recoverability, while performance-based metrics generally quantify how resilient a power system is in the event of HILF disruptions. To explore power grid attributes, complex network theory and methods are widely utilized [12], [33]–[36], in which power grid is analyzed from the aspect of graph and connection. But only network-based index may not fully reflect power system resiliency. It is more desirable to combine network-related index with operation-based indices so as to take advantage of both methods and reflect power system resiliency all around. To

synthesize multiple resiliency indicators, which could be more convenient to read and utilize, multicriteria decision making theory is commonly used [3], [37], [38].

In this article, a set of multivariable resiliency metric is used to quantify distribution grid resiliency and help select a strategy to maximize resiliency. Metrics and process to maximize resiliency using metrics given alternative strategy is incorporated in the RT-RMS tool as introduced in Section V. The value of the metric enables operators to compare the proposed "resiliency operation strategy" with "economical operation strategy" intuitively in the RT-RMS tool. The developed resiliency metric consists of five factors from both network and operation aspects. Specifically, $\vec{R} = [\text{Grap}, \text{EIM}, \text{CLD}, \text{CLNL}, \text{TG}]$[12], [39]. And the positive or negative influence of each factor on the composite score is designated by $+1$ and -1.

1) Geographical metrics (Grap)$(+1)$. Power grid can be represented by a graph $G = (N, E, W)$, where N is the node set, consisting of node names of power grid; E stands for the edge set, with each element $E(i, j)$ indicates a branch from node $'i'$ to node $'j'$; and W represents weight set of branches or loads. In this article, W is one-to-one correspondent to nodes set N, indicating the importance of loads. In this work, loads are characterized into three importance levels, while $'1'$ indicates the most critical load, $'2'$ and $'3'$ represent the less important loads. Geographical metrics reflect power grid structural properties as a graph. Following geographical factors are used in this work, which can be represented as Grap $= [\text{Dia}, K, \lambda_2, BC_{\text{agg}}]$:

1) Diameter Dia$(+1)$: Dia=maxE(i,j)
2) Average length of edges $K(+1)$

$$K = \frac{2\,|E|}{|N|\,(|N|-1)}$$

which indicates the average path length

3) Algebraic connectivity $\lambda_2(+1)$: λ_2 is the second smallest eigenvalue, indicates the connectivity status of the network.
4) Aggregate betweenness centrality $BC_{\text{agg}}(-1)$:

$$\text{BC}_{\text{agg}} = \frac{1}{N}\sum_{k=1}^{N}\deg(k)\sum_{i\neq j}\frac{\sigma_{ij}(k)}{\sigma_{ij}}$$

where $\deg(k)$ is the degree of kth node, and $\sigma_{ij}(k)$ means the number of shortest paths between node *i* and *j* passing through node k. Therefore, BC_{agg} shows the aggregated centrality of a power grid.

2) Event impact metric (EIM)(-1): This is a set of predefined values for various event scenarios. Since possible events and influence for different locations vary significantly, it is impossible to apply a set of values to all scenarios. Here, they are input as empirical values defined subjectively by operators. EIM should be set specifically according to the geographical arrangement of a power grid. The higher it is set, the more serious the event may affect the power system, the more challenging it is for the power system to withstand.
3) Critical load demand (CLD)$(+1)$: CLD indicates the total critical load demand capacity not affected by events. Higher CLD indicates smaller influence the event bring to the power grid.
4) Critical load not lost (CLNL)$(+1)$: CLNL indicates the proportion of critical load remain in operation.
5) Total generation (TG)$(+1)$: This factor indicates total generation capacity available for dispatching during the event.

The overall geographical metric score and the comprehensive resiliency score are obtained by analytical hierarchical process (AHP). For either geographical metrics or overall resiliency metrics, not all metrics are equally important for indicating resiliency score, so AHP is applied to derive weights vector $\vec{V}$, indicating relative importance of factors. For the multicriteria vector $\vec{R}$ that weights are to be derived, a pairwise comparison matrix (PCM) $A = [a_{ij}]_{m\times m}$ is created as shown in (1), whose dimension $m \times m$ equals to the number of factors, and the entries a_{ij} correspond to their relative importance. The PCM entries are formulated by careful considering the relative importance of each factor, and standardized scale is used here to create a stringent band of preference. For example, to derive weights for resiliency metrics

$$\vec{R} = [\text{Grap}, \text{EIM}, \text{CLD}, \text{CLNL}, \text{TG}]$$

1/a indicates the influence of factor EIM is 1/a times that of $Grap$. Specifically, the values of PCM entries are defined within following criteria: 1-equal; 3-weak; 5-strong; 7-significant; 9-absolute; no intermediate values allowed. Besides, the consistency of weights derived from PCM matrix is checked by consistency ratio, which is kept below 10%. The detailed calculation method could be found in [40]. By complying with a standardized scale and consistency ratio check, the consistency of weights derived is guaranteed. Then, the weights vector $\vec{V}$ in correspondence with the resiliency metrics vector is obtained as the dominant eigenvector of the PCM

$$A = \begin{bmatrix} 1 & a & b & c & d \\ 1/a & 1 & e & f & g \\ 1/b & 1/e & 1 & h & i \\ 1/c & 1/f & 1/h & 1 & j \\ 1/d & 1/g & 1/i & 1/j & 1 \end{bmatrix}. \tag{1}$$

Since entries in resilience vector are scaled by different units, they need to be normalized before synthesized. Take the resilience vector of normal power grid status as a reference, let $\rho(i, j)$ be an element of resilience vector, depending on the positive or negative influence of $\rho(i, j)$ has on the resilience score, it is normalized with following equations. For positive influence factor

$$\rho(i,j)' = \frac{\rho(i,j) - \min_{j=1}^{n}(\rho(i,j))}{\max_{j=1}^{n}(\rho(i,j)) - \min_{j=1}^{n}(\rho(i,j))}. \tag{2}$$

For negative influence factor

$$\rho(i,j)' = \frac{\max_{j=1}^{n}(\rho(i,j)) - \rho(i,j)}{\max_{j=1}^{n}(\rho(i,j)) - \min_{j=1}^{n}(\rho(i,j))} \tag{3}$$

where n indicates the number of resiliency metrics elements. Therefore, the composite resiliency score of the power grid for a specific scenario is obtained by

$$R = \sum_{j=1}^{n} V_j \rho(i,j)'. \tag{4}$$

III. Economic and Resilience Operation Mode

For islanded hydro–diesel-battery microgrid, small hydropower plants (SHPs) are usually run-of-river without or only with limited water storage. The maximum output capacity of this kind of generation is largely dependent on seasonal river flows, so the output of SHPs is not constant and may not be a reliable source to meet load demand during peak load hours and during abnormal winter freezing periods. Since microgrid is isolated from large power system, it is challenging to keep power system frequency stable, and requires stringent actions to regulate the frequency within boundaries. In order to achieve this, a certain generation capacity has to be reserved for frequency regulation. In hydro-only mode, generation capacity is reserved by diverting part of the river flow away from generation, which could be a waste of generation resources. In general, the generation cost of SHPs is the lowest compared with other forms of production, hence it is preferred to take advantage of SHPs generation first. On the other hand, the generation cost of diesel generators (DGs) is much higher, around 10 times than that of SHPs, depending on diesel price. Besides, due to minimum output constraints for DGs, it is very uneconomical to start DGs and divert river flows when the generation gap to be filled is small to meet frequency regulation requirements. So, the installment of BESS can reduce generation costs, improve operational flexibility, and resilience significantly. Resilience operation mode of hydro–diesel-battery microgrid is introduced in [39]. In this work, a detailed resilience-driven coordination strategy for islanded hydro–diesel-battery microgrid is proposed.

The operation steps and switching between economical and resilience mode are demonstrated in Fig. 1. During normal operation status, the microgrid operates under economical mode. It is preferable to take advantage of SHPs, and to minimize the output from DGs. The activation of resiliency-mode depends on weather prediction information. While event prediction arrives, BESS is expected to turn into charging mode and fully charge before the event. The effectiveness of this proposed resilience operation strategy under HILF events is evaluated through the resilience metric explained in Section II, and the power output of various resources is set correspondingly. Assume an event strikes power grid at $t_0 = T_{\text{event}}$, and at $t_{-1} = T_{\text{event}} - h$, event alert is received. Define event alert in (5)

$$\begin{cases} \text{Alert} = 0, t < T_{\text{event}} - h \\ \text{Alert} = 1, t \geq T_{\text{event}} - h \end{cases}. \tag{5}$$

The dispatch of the microgrid generators in normal operation can be summarized into following scenarios by different level of load demand, SOC and SHPs:

1) Hydroelectricity is enough to supply load and reserve capacity demand, while $\text{SOC}^{\min} \leq \text{SOC} \leq \text{SOC}^{\max}$, Alert $= 0$.
2) Only coordination of SHPs and BESS are enough to supply load and reserve capacity demand, while $\text{SOC}^{\min} \leq \text{SOC} \leq \text{SOC}^{\max}$, Alert=0.
3) Load and reserve demand is greater than the maximum power can be supplied by SHPs and BESS, while $\text{SOC}^{\min} \leq \text{SOC} \leq \text{SOC}^{\max}$, Alert=0.
4) For above power demand conditions, suppose BESS is not available for power supply($\text{SOC} \leq SOC^{min}$) or Alert=1.

The proposed resource coordination algorithm is formulated as a quadratic programming problem with linear constraints, as shown in (6)–(17) The first two terms of (6) indicate the cost of hydro and DGs, and the third term represents the cost relating to charging/discharging of BESS, which are virtual costs but not real physical costs. The virtual cost of BESS C_{BSi} should be set between the cost of SHP C_{Hi} and the cost of DGs C_{Di}, so that BESS is prioritized over DGs when SHP generation is not enough. The charging/discharging indicators are binary variables determined by SOC and Alert status as shown in Fig. 1. Usually, a certain amount of power P_{Ri} is reserved for frequency control. Therefore, in this article, we assume the reserved power capacity is enough to keep frequency stable, the frequency control strategy is not considered in this work. Generation capacity of hydro and DGs are presented in (10) and (11). Line limit is shown in (13). Charging/discharging rate limit of BESS are shown in (14) and (15). SOC limit and calculation of BESS are presented in (16) and (17). Sensitivity approach combined with load flow calculated by OpenDSS is used to make sure that line currents and bus voltages are considered in constraints [29]. Compared with traditional AC OPF, sensitivity approach could substantially reduce computational complexity in a practical way, and therefore, it is more suitable for real-time application. The equations for line current and voltage limits (8) and (9) are not included in the optimization model until line current/bus voltage constraints violations are observed in load flow analysis. The sensitivity matrices are derived according to the difference between power flow solutions under the base case and the case with control variable perturbation. Equation (12) is the model for voltage regulator. Assume 32-step VRs with voltage regulation range of $\pm 10\%$ are used, then a_ϕ range between $0.9 - 1.1\text{p} \cdot \text{u}$. and each step results in a voltage change of $0.00625\ \text{p} \cdot \text{u}$.

$$\begin{aligned} F = & \sum_{Hi} C_{Hi}(t) P_{Hi}(t) + \sum_{Di} C_{Di}(t) P_{Di}(t) \\ & + \sum_{\text{BSi}} C_{\text{BSi}}(t) \cdot [Id^d_{\text{BSi}}(t) P^d_{\text{BSi}}(t) \eta_d \\ & - Id^c_{\text{BSi}}(t) P^c_{\text{BSi}}(t) \eta_c] \end{aligned} \tag{6}$$

Constraints

$$\begin{aligned} & \sum_{Hi} P_{Hi}(t) + \sum_{Di} P_{Di}(t) + \sum_{\text{BSi}} (P^d_{\text{BSi}}(t)\eta_d - P^c_{\text{BSi}}(t)\eta_c) \\ & = P_L(t) + P_R \end{aligned} \tag{7}$$

$$I_l^{\text{pre}} + \sum_{u=1}^{n_u} S_u^{I_l} * \Delta u \leq I_l^{\max}, l = 1, \ldots, n_l \tag{8}$$

$$V_n^{\min} \leqslant V_n^{\text{pre}} + \sum_{u=1}^{n_u} S_u^{V_n} * \Delta u \leq V_n^{\max}, n = 1, \ldots, N_{\text{bus}} \tag{9}$$

$$P_{Hi}^{\min} \leqslant P_{Hi}(t) \leqslant P_{Hi}^{\max} \tag{10}$$

$$P_{Di}^{\min} \leqslant P_{Di}(t) \leqslant P_{Di}^{\max} \tag{11}$$

$$V_j^{\phi} = a_{\phi} V_i^{\phi}, \phi = 1, \ldots, n_{\phi} \tag{12}$$

$$P_{ij} \leqslant P_{ij}^{\max} \tag{13}$$

$$0 \leqslant P_{Bi}^{d}(t) \leqslant P_{Bd}^{\max} \tag{14}$$

$$0 \leqslant P_{Bi}^{c}(t) \leqslant P_{Bc}^{\max} \tag{15}$$

$$\text{SOC}^{\min} \leqslant \text{SOC}_{Bi}(t) \leqslant \text{SOC}^{\max} \tag{16}$$

$$\text{SOC}_{Bi}(t) = \text{SOC}_{Bi}(t-1) + (P_{Bi}^{c}(t)\eta_c - P_{Bi}^{d}(t)\eta_d) \cdot \Delta t. \tag{17}$$

Variables in above mathematical model are updated every time interval Δt. Notations used in (6)–(17) are explained as follows:

Hi, Di, BSi hydro, DG, and BESS unit.
C_{Hi} generation cost of hydro unit.
C_{Di} generation cost of diesel unit.
C_{BSi} virtual BESS discharging/charging cost.
P_{hi}, P_{Di} hydro, diesel unit active power generation.
P_{BSi}^{d}, P_{BSi}^{c} BESS unit discharging/charging power.
P_{ij} distribution line flow.
$Id_{BSi}^{d}, Id_{BSi}^{c}$ BESS unit discharging/charging status, which are binary variables, ON/OFF=1/0.
a_{ϕ} turn ratio for the VR connected to phase ϕ of line (i, j).
SOC_{Bi} status of charge of BESS unit.
k, N_{bus} node number, total number of nodes.
$I_l^{\text{pre}}, V_n^{\text{pre}}$ current/voltage magnitude in previous interval.
$S_u^{I_l}, S_u^{V_n}$ line current/node voltage sensitivity matrix with respect to control variables.
$u, \Delta u$ control variable and its deviation, which is the voltage difference caused by voltage regulator.
$V_n^{\min}, V_n^{\max}$ node voltage lower/upper limit.
$I_l^{\max}$ line current limit.
P_{Li}, P_{Ri} load demand and reserve capacity demand.
$P_{Hi}^{\min}, P_{Hi}^{\max}$ lower and upper limit of hydro unit generation.
$P_{Di}^{\min}, P_{Di}^{\max}$ lower and upper limit of diesel unit generation.
$P_{ij}^{\max}$ maximum line flow constraint.
$P_{Bd}^{\max}, P_{Bc}^{\max}$ maximum discharging/charging rate of BESS.
$\text{SOC}^{\min}, \text{SOC}^{\max}$ lower and upper limit of SOC of BESS unit.
Δt length of time interval.

IV. Case Study and Simulation Results

The proposed strategy is tested in two test cases: one revised 14-node test case and one real world 55-node test case representing isolated microgrid system. Scenarios developed in a 14-node test case verify the sensitivity of proposed strategy to different load levels under normal conditions, and the improvement of resilience operation mode over economical operation mode under an event. In 55-node test case, besides analysis of system performance under economical mode and resilience mode, resilience scores are calculated to quantify the benefits that resilience operation mode brought about to system.

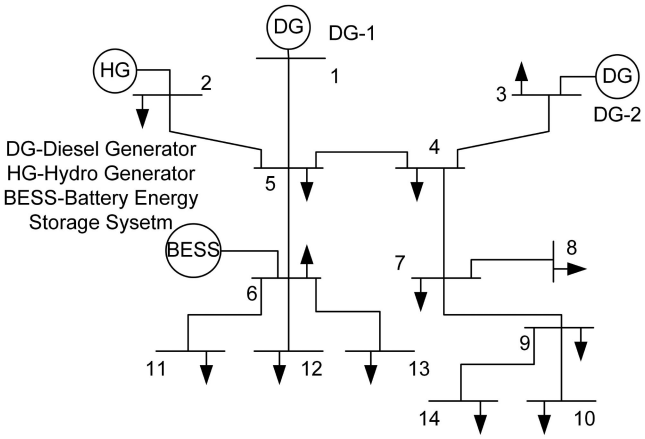

Fig. 2. One-line-diagram of 14-node system.

TABLE II
Parameters of Generators in the 14-Node System

type	Location	Pmax(kW)	Pmin(kW)
Hydro	node-2	300	50
Diesel	node-1,3	200	35

TABLE III
Parameters of BESS Unit in the 14-Node System

Type	BESS
Location	node-6
Maximum charging rate (kW)	-50
Maximum discharging rate (kW)	50
Maximum energy capacity (kWh)	300
Minimum energy capacity (kWh)	90
Charging efficiency (%)	85
Discharging efficiency(%)	85

A. Revised 14 Node Test Case

A modified 14-node system is used to validate the proposed islanded microgrid resource coordination strategy. Four distributed generators are added to the system, including two DGs, one hydro generator (HG), and one BESS. The one-line-diagram of the modified 14-node system is shown in Fig. 2, parameters of generators and BESS are showed in Tables II and III. Generation cost of each type of generation resource is given in (18)–(20). As explained previously, the cost relating to battery is virtual, and assumed between the generation cost of hydro and diesel

$$\text{Hydro} : F(P) = 0.000162P^2 + 1.92P + 78 \tag{18}$$

$$\text{Diesel} : F(P) = 0.0094P^2 + 5.85P + 210 \tag{19}$$

$$\text{Battery} : F(P) = 0.0012P^2 + 4.27P + 150. \tag{20}$$

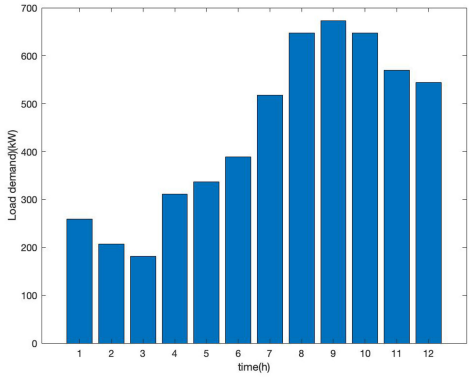

Fig. 3. Load profile-case 1 scenario 1.

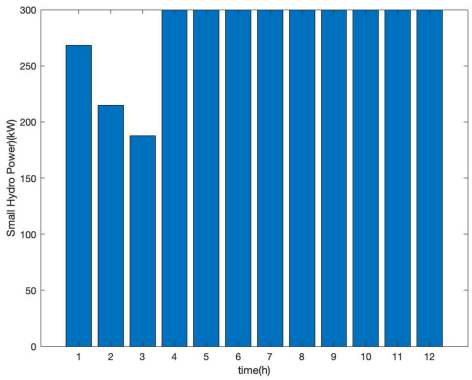

Fig. 4. Hydro output power-case 1 scenario 1.

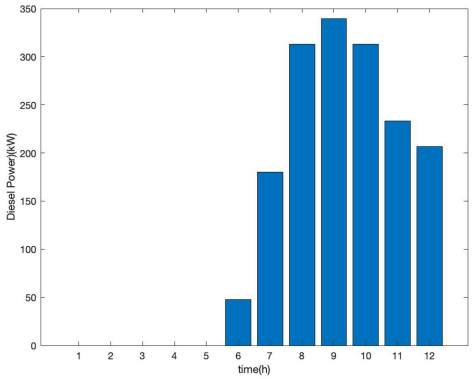

Fig. 5. Diesel output power-case 1 scenario 1.

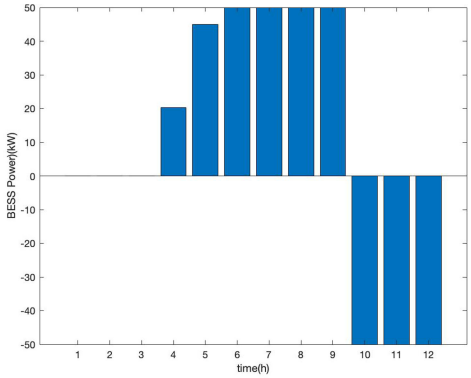

Fig. 6. BESS output power-case 1 scenario 1.

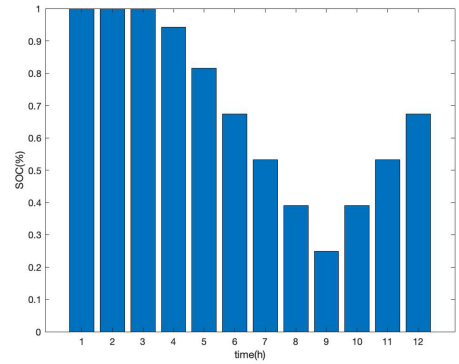

Fig. 7. SOC-case 1 scenario 1.

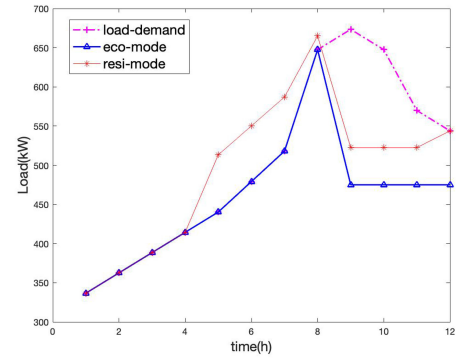

Fig. 8. Load profile-case 1 scenario 2.

In this test case, two scenarios are developed: scenario 1 illustrates system performance during normal operation, the sensitivity of proposed strategy for different load levels, and scenario 2 compares system performance under an event when in economical mode and resilience mode, respectively. In scenario 1, Fig. 3 shows the load profile, and Figs. 4–6 show output of HG, DG, and BESS, respectively, while Fig. 7 shows the status-of-charge of BESS, which starts from 100%. During hour 1–3, the load demand is low and power supply only comes from HGs; while in hour 4–5, load demand is met by HGs and BESS coordinately; during hour 6–12, load demand is higher than the maximum capacity of BESS and hydropower plant, so DG is participating in power supply. At hour-9, SOC of BESS reaches the lowest boundary and therefore is charged during hour 10–12.

In scenario 2, assume DG-2 quit at hour-9 because of an event, and the event alert is received at hour-4. To compare the performance of resilience-mode and economical-mode more effectively, load demand is always set at a higher level, which requires the coordination of hydro–diesel-BESS, as shown in Fig. 8. Here, "eco-mode" and "resi-mode" indicate power supplied under two operation modes, respectively. In hour 4–9, "resi-mode" power supply is higher than "eco-mode" because battery was charged since event alert comes at hour-4. During hour 9–12, power demand is higher than the total power supply capacity of the system, part of load has to be shed. However, "resi-mode" could supply more load than "eco-mode" because

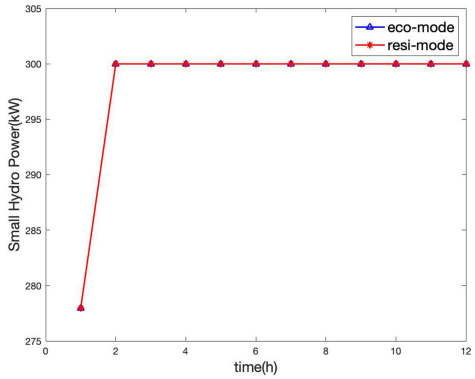

Fig. 9. Hydro output power-case 1 scenario 2.

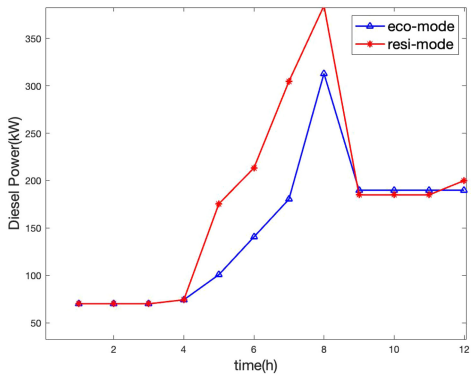

Fig. 10. Diesel output power-case 1 scenario 2.

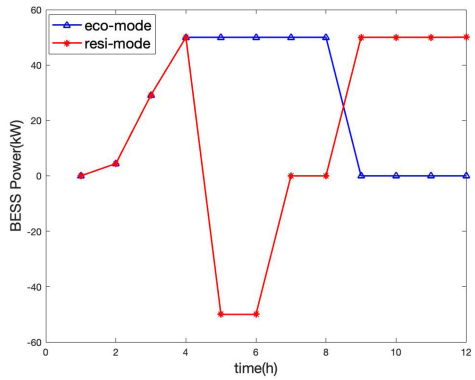

Fig. 11. BESS output power-case 1 scenario 2.

BESS was fully prepared. The power of BESS and SOC condition are shown in Figs. 11 and 12. During hour 4–6, BESS is fully charged and is held on not supplying power until event happens at hour-9. In contrast, the charging status of BESS is not influenced by event alert signal, and keep supplying power before event happens at hour-9 under "eco-mode." During hour 9–12, SOC has reached the lowest boundary, and since the total online generation capacity is not enough to meet all load demand, BESS is not charged during event. The power output of hydro and DGs are shown in Figs. 9 and 10. At hour-1, load demand is supplied by HG and DGs, constrained by the minimum output of DG, hydropower is not fully used. For other time, HG operates at highest capacity. During hour 4–9, diesel generation is higher in "resi-mode" than "eco-mode," because BESS is charged during

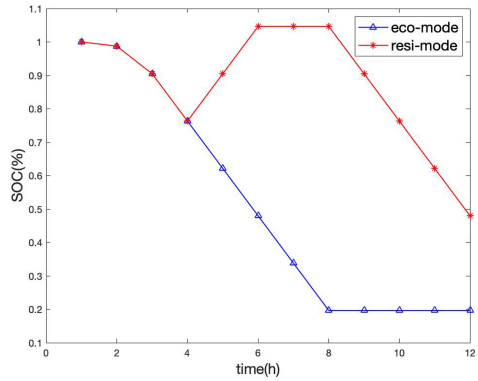

Fig. 12. SOC-case 1 scenario 2.

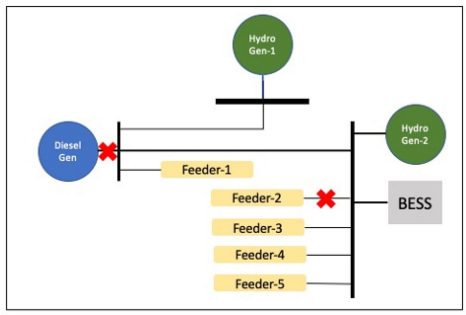

Fig. 13. Simplified Microgrid System with hydro–diesel-battery.

TABLE IV
HYDRO–DIESEL-BATTERY MICROGRID CONFIGURATION

C_{diesel}	C_{Hydro1}	C_{Hydro2}	$maxP^{out}_{BESS}$	$P_{reserve}$	P_{Load}
10.8MW	1.25MW	6.0MW	1.0MW	0.75MW	9.025MW

this period. During hour 9–12, since DG-2 is out of power, only DG-1 operates during the event.

B. 55-Node Islanded Microgrid Test Case

A real hydro–diesel-battery microgrid is modeled for simulation, as shown in Fig. 13 and Table IV. Assume tsunami event strikes this system at T, which leads to the outage of feeder-2, and diesel power plant tripping from operation. Also assume distribution grid information, event prediction, SOC of BESS, etc., are updated every time interval. Suppose alert of event from weather prediction platform was detected three time intervals before the event strike, which is at $T-3$. In economic mode, the generation dispatch strategy does not change when event alert is observed, which means the microgrid keeps following economical operation strategy during $(T-3)-T$. Whereas in resiliency mode, the microgrid follows the generation strategy described in Fig. 1, and BESS is checked and fully charged before the event occurs at T.

The state of charge of BESS when the microgrid operates under resilience mode and economical mode are shown in Table V and Fig. 14. In economical mode, when tsunami event alert is received at $T-3$, generation strategy is not adjusted, and therefore BESS continues to supply load in the following hours. When an event occurs at T, only 10% of energy of BESS is left, and soon BESS is not available for power supply, since

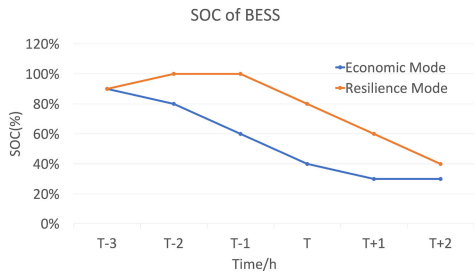

Fig. 14. SOC of BESS given tsunami strike at t=T.

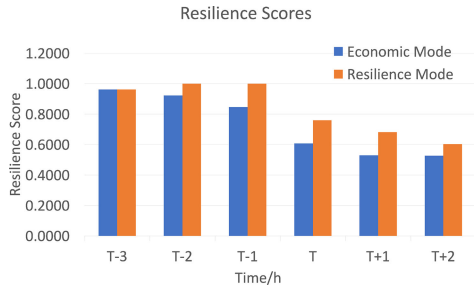

Fig. 15. Resilience Scores given tsunami strike at t=T.

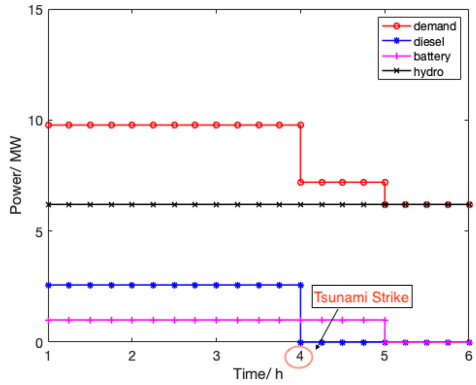

Fig. 16. Generation dispatch in economic mode.

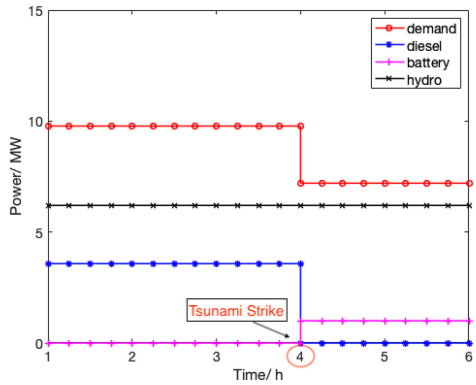

Fig. 17. Generation dispatch in resilience mode.

TABLE V
COMPARISON OF SOC FOR ECONOMICAL AND RESILIENCE MODE

SOC	T-3	T-2	T-1	T	T+1	T+2
E-mode	90%	80%	60%	40%	30%	30%
R-mode	90%	100%	100%	80%	60%	40%

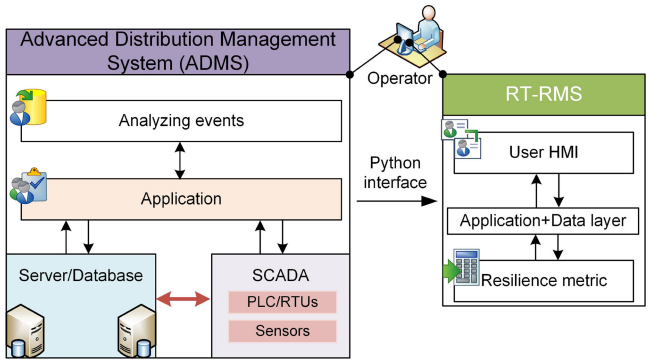

Fig. 18. Representative architecture of RT-RMS tool interfacing with ADMS.

TABLE VI
COMPARISON OF RESILIENCE SCORES FOR ECONOMICAL AND RESILIENCE MODE

Resilience	T-3	T-2	T-1	T	T+1	T+2
E-mode	0.9617	0.9233	0.8469	0.6080	0.5296	0.5274
R-mode	0.9617	0.9994	0.9991	0.7603	0.6819	0.6035

SOC reaches the minimum limit. While in resilience mode, once event alert is detected at $T-3$, BESS stops discharging and turns into charging mode. And when event occurs at T it has been fully charged. The generation dispatch of various resources during simulation intervals is shown in Figs. 16 and 17. Suppose actual total output of hydro plants is $P_{\text{hydro}} = 6.2$ MW and keeps constant. At $T = 1$, since tsunami event alert is detected, in resilience mode BESS is charged to maximum storage, while in economic mode BESS continue to supply power to load; at $T = 4$, DGs tripped because of tsunami and part of load has to be shed. In economic mode, BESS stops discharging at $T = 5$, because SOC drops to the minimum limit, and more load has to be shed. In comparison, however, in resilience mode more load can be supplied for a longer time because BESS has been fully charged before event occurs.

The resilience scores are shown in Table VI and Fig. 15. Resilience scores are effectively improved when the microgrid is dispatched in resilience mode.

V. INTEGRATING RESILIENCY COMPUTATION TOOL WITH ADMS

Resilience metric with detailed formulation presented in previous sections is considered as key input in developing the RT-RMS tool. Integration of RT-RMS with advanced distribution management system (ADMS) is depicted in Fig. 18, for real-world application. A layered structure of ADMS software platform is displayed in Fig. 18 to embrace its basic functional blocks and also software layers. In Fig. 18, the top layer comprises of user/client interface to fetch the current system information from applications via database. The middle layer accommodates various prime applications (power flow analysis (PFA), fault location (FL), node load allocation (NLA), reconfiguration, volt-var management (VVM), etc.) to execute, and results are written back to the database with time stamping and triggering index. The bottom layer encloses key elements of

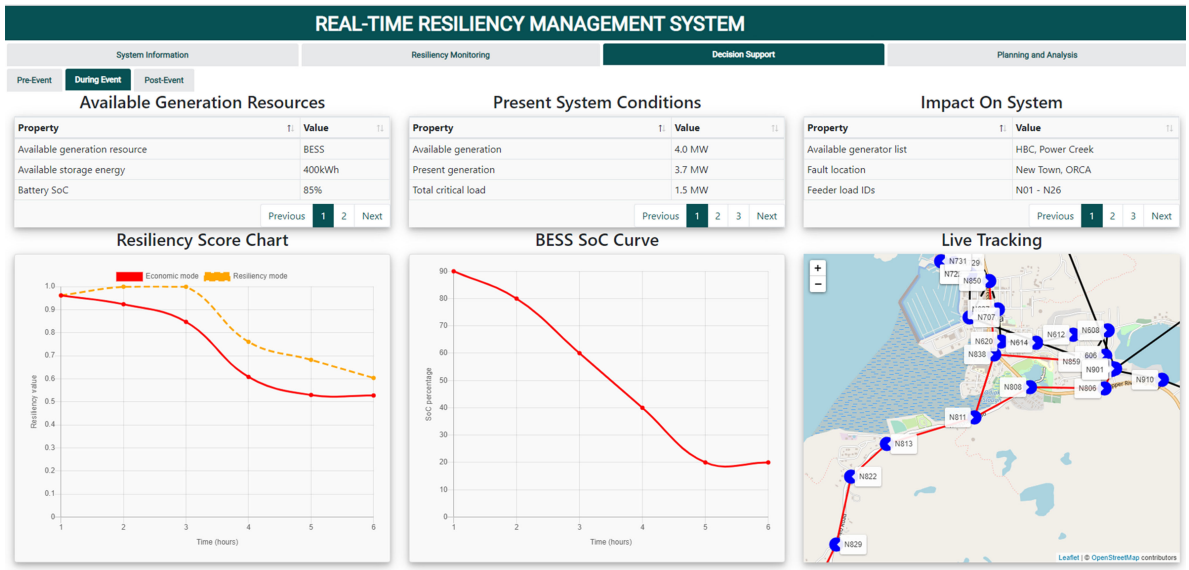

Fig. 19. Visualizing a practical case study using the RT-RMS.

ADMS namely, server, and SCADA, which provides data storage, real-time monitoring, data acquisition, and device control platforms through which real time data exchange and control commands are performed.

RT-RMS encloses three major functional layers and is labeled as user human–machine interface (HMI), intermediate application layer, and resilience metric. All user queries and requested case scenario analysis are performed through user HMI. Queries and requested studies are structured in the intermediate application layer and it also links appropriate data sets received from ADMS to core resilience metric with fixed periodicity. Resilience score computations are executed using detailed formulation and procedures furnished in Sections II and III. Complete RT-RMS tool development methodology and assembling process is illustrated in [41]. Python interface is used to establish the communication between ADMS and RT-RMS tool, and also provides a platform to exchange information between them. RT-RMS tool explicit integration does not alter the existing ADMS functionalities and helps the operator to consider a most resilient solution in case of emergencies, including three stages of the event (i.e., pre-, during, and postevent). Detailed solutions for three stages of the event is out of the work scope in this article. However, similar work can be found in [42].

As shown in Fig. 19, RT-RMS dashboard consists of four tabs that cover as-built model information of the system, real-time resiliency monitoring, decision support, and planning and analysis. First tab provides details of the planned network model with inbuilt power system components, controllers, measurement, and communication devices, etc. Here, the system data does not change until as-built model is modified through expansion and plugging of more customers and resources. Second tab assess system present condition with respect to different resilience factors discussed in Section II and furnishes current resilience score according to available resources information, generation, and load demand values. Third tab includes decision support against three stages of threat with the help of proactive reconfiguration plans, and preplanned dispatch of resources, and quick restoration schemes. On the last tab, long-term planning analysis window is provided to conduct the system value benefits to avail maximum resilience through minimal additions of backup generation facilities, smart sensors, and controllers, AMIs, high resolution data recording facilities.

A practical distribution system with HILF threat scenario is considered for demonstration of RT-RMS tool usefulness, and details of the test utility network are concealed to preserve privacy from utility perspective. A screenshot of the tool with a real case scenario is disclosed in Fig. 19. Tsunami threat scenario is applied to test utility network and its real impact on system during event stage is detailed in tabular form as shown in Fig. 19. Resilience score is calculated using contributing factors (i.e., with the help of Sections II and III) and associated score (i.e., given in Section IV-B) reveals the advantage of preserving the energy storage system before event to provide more sustained power supply to critical loads as shown in Fig. 19. A quick action plan is available to the operator for immediate support that helps in improving the resiliency of system.

VI. Conclusion

In this work, a detailed proactive energy resource coordination strategy for an islanded hydro–diesel-battery microgrid is proposed to increase resiliency performance under extreme events. The sensitivity analysis of the proposed strategy is performed in a modified 14-node isolated power system model under normal operation as well as during extreme conditions. Also, the testing and validation of the proposed strategy are performed in a real-world 55-nodes islanded hydro–diesel-battery microgrid when impacted by a tsunami event. RT-RMS, a real-time resilience monitoring and management platform, is developed to help the operator for decision making. The proposed resources dispatch strategy is integrated within the RT-RMS for economic and resilient operations. The case study results indicate that the proposed proactive resource coordination strategy could effectively improve the microgrid resilience performance during extreme events.

ACKNOWLEDGMENT

Technical support from C. Koplin, R. Hovsapian and M. Panwar is greatly appreciated.

REFERENCES

[1] E. Sandoval, R.Rojas, and A. Waller, "Death Toll from Texas. Winter Storm Rises Sharply to 111," Accessed: Mar. 25, 2021. [Online]. Available: https://www.nytimes.com/topic/subject/power-failures-and-blackouts

[2] C. S. Holling, "Resilience and stability of ecological systems," *Annu. Rev. Ecol. Systematics*, vol. 4, no. 1, pp. 1–23, 1973.

[3] M. Panteli, P. Mancarella, D. N. Trakas, E. Kyriakides, and N. D. Hatziargyriou, "Metrics and quantification of operational and infrastructure resilience in power systems," *IEEE Trans. Power Syst.*, vol. 32, no. 6, pp. 4732–4742, Nov. 2017.

[4] National Academies of Sciences, *Enhancing the Resilience of the Nation's Electricity System*. Washington, DC, USA: National Academies Press, 2017.

[5] H. Aki, "Demand-side resiliency and electricity continuity: Experiences and lessons learned in Japan," *Proc. IEEE Proc. IRE*, vol. 105, no. 7, pp. 1443–1455, Jul. 2017.

[6] J.-P. Watson *et al.*, "Conceptual framework for developing resilience metrics for the electricity oil and gas sectors in the United States," Sandia National Laboratories, Albuquerque, NM (*United States), Tech. Rep. SAND2014-18019*, 2014.

[7] E. D. Vugrin, A. R. Castillo, and C. A. Silva-Monroy, "Resilience metrics for the electric power system: A performance-based approach," *Sandia National Lab. (SNL-NM)*, Albuquerque, NM (United States), Tech. Rep. SAND2017-1493, 2017.

[8] N. K. Carrington, I. Dobson, and Z. Wang, "Extracting resilience metrics from distribution utility data using outage and restore process statistics," *IEEE Trans. Power Syst.*, vol. 36, no. 6, pp. 5814–5823, 2021.

[9] M. Panteli, D. N. Trakas, P. Mancarella, and N. D. Hatziargyriou, "Power systems resilience assessment: Hardening and smart operational enhancement strategies," *Proc. IEEE*, vol. 105, no. 7, pp. 1202–1213, Jul. 2017.

[10] A. Arjomandi-Nezhad, M. Fotuhi-Firuzabad, M. Moeini-Aghtaie, A. Safdarian, P. Dehghanian, and F. Wang, "Modeling and optimizing recovery strategies for power distribution system resilience," *IEEE Syst. J.*, vol. 15, no. 4, pp. 4725–4734, Dec. 2021.

[11] N. Bhusal, M. Abdelmalak, M. Kamruzzaman, and M. Benidris, "Power system resilience: Current practices, challenges, and future directions," *IEEE Access*, vol. 8, pp. 18064–18086, 2020.

[12] S. Chanda and A. K. Srivastava, "Defining and enabling resiliency of electric distribution systems with multiple microgrids," *IEEE Trans. Smart Grid*, vol. 7, no. 6, pp. 2859–2868, Nov. 2016.

[13] W. Feng *et al.*, "A review of microgrid development in the United States-A decade of progress on policies, demonstrations, controls, and software tools," *Appl. Energy*, vol. 228, pp. 1656–1668, 2018.

[14] X. Duan, S. Wu, R. Diao, and A. Yang, "Design of hybrid solar-hydro microgrid for village school in China," in *Proc. IEEE Glob. Humanitarian Technol. Conf.*, 2018, pp. 1–7.

[15] M. Sufyan, N. A. Rahim, C. Tan, M. A. Muhammad, and S. R. S. Raihan, "Optimal sizing and energy scheduling of isolated microgrid considering the battery lifetime degradation," *PLos One*, vol. 14, no. 2, pp. 1–28, 2019.

[16] I. Alsaidan, A. Khodaei, and W. Gao, "A comprehensive battery energy storage optimal sizing model for microgrid applications," *IEEE Trans. Power Syst.*, vol. 33, no. 4, pp. 3968–3980, Jul. 2018.

[17] M. R. Aghamohammadi and H. Abdolahinia, "A new approach for optimal sizing of battery energy storage system for primary frequency control of islanded microgrid," *Int. J. Elect. Power Energy Syst.*, vol. 54, pp. 325–333, 2014.

[18] H. Khorramdel, J. Aghaei, B. Khorramdel, and P. Siano, "Optimal battery sizing in microgrids using probabilistic unit commitment," *IEEE Trans. Ind. Informat.*, vol. 12, no. 2, pp. 834–843, Apr. 2016.

[19] Y. Sawle, S. Jain, S. Babu, A. R. Nair, and B. Khan, "Prefeasibility economic and sensitivity assessment of hybrid renewable energy system," *IEEE Access*, vol. 9, pp. 28260–28271, 2021.

[20] J. Zhang, X. Shao, Y. Li, J. Lin, F. Li, and Z. Zhang, "Research on frequency regulation strategy based on model predictive control for wind-hydro-storage complementary microgrid," in *Proc. 4th Int. Conf. HVDC*, 2020, pp. 1031–1036.

[21] Y. Guan, J. C. Vasquez, J. M. Guerrero, Y. Wang, and W. Feng, "Frequency stability of hierarchically controlled hybrid photovoltaic-battery-hydropower microgrids," *IEEE Trans. Ind. Appl.*, vol. 51, no. 6, pp. 4729–4742, Nov./Dec. 2015.

[22] C. Marinescu and I. Serban, "Robust frequency control for a wind/hydro autonomous microgrid," in *Proc. IEEE Trondheim PowerTech*, 2011, pp. 1–6.

[23] J. Xiao, L. Bai, F. Li, H. Liang, and C. Wang, "Sizing of energy storage and diesel generators in an isolated microgrid using discrete fourier transform (DFT)," *IEEE Trans. Sustain. Energy*, vol. 5, no. 3, pp. 907–916, Jul. 2014.

[24] G. Pathak, B. Singh, and B. K. Panigrahi, "Wind-hydro microgrid and its control for rural energy system," *IEEE Trans. Ind. Appl.*, vol. 55, no. 3, pp. 3037–3045, May/Jun. 2019.

[25] J. Li, S. Wang, L. Ye, and J. Fang, "A coordinated dispatch method with pumped-storage and battery-storage for compensating the variation of wind power," *Protection Control Modern Power Syst.*, vol. 3, no. 1, pp. 1–14, 2018.

[26] A. M. Abdulmohsen, M. A. El-Sharkawy, and W. A. Omran, "Power management in islanded microgrids using multi-agent systems," in *Proc. IEEE PES Innov. Smart Grid Technol. Conf. Europe*, 2016, pp. 1–6.

[27] T.-H. Kim, H.-S. Shin, H.-T. Kim, S.-W. Lee, and W. Kim, "A multi-period optimal power flow algorithm for microgrid in consideration with the state-of-charge of BESS's," in *Proc. IEEE Transp. Electrific. Conf. Expo, Asia-Pacific*, 2016, pp. 635–640.

[28] H. Saitoh, M. Abe, and W. Yashima, "A proposal of emergency microgrid operation of distribution systems after large scale disasters," in *Proc. IEEE Region 10 Humanitarian Technol. Conf.*, 2013, pp. 136–141.

[29] F. Yang, X. Feng, and Z. Li, "Advanced microgrid energy management system for future sustainable and resilient power grid," *IEEE Trans. Ind. Appl.*, vol. 55, no. 6, pp. 7251–7260, Nov./Dec. 2019.

[30] M. Göransson, N. Larsson, L. A. Tuan, and D. Steen, "Cost-benefit analysis of battery storage investment for microgrid of Chalmers university campus using μ-OPF framework," in *Proc. IEEE Manchester PowerTech*, 2017, pp. 1–6.

[31] R. Jamalzadeh and M. Hong, "Microgrid optimal power flow using the generalized benders decomposition approach," *IEEE Trans. Sustain. Energy*, vol. 10, no. 4, pp. 2050–2064, Oct. 2019.

[32] J. Linli, K. Gowtham, P. Sanjeev, and S. Anurag, "Coordinating energy resources in an islanded microgrid for economic and resilient operation," in *Proc. IEEE Ind. Appl. Soc. Annu. Meeting*, 2021, pp. 1–7.

[33] A. M. Amani and M. Jalili, "Power grids as complex networks: Resilience and reliability analysis," *IEEE Access*, vol. 9, pp. 119010–119031, 2021.

[34] P. Dehghanian, S. Aslan, and P. Dehghanian, "Maintaining electric system safety through an enhanced network resilience," *IEEE Trans. Ind. Appl.*, vol. 54, no. 5, pp. 4927–4937, Sep./Oct. 2018.

[35] P. Bajpai, S. Chanda, and A.K. Srivastava, "A novel metric to quantify and enable resilient distribution system using graph theory and choquet integral," *IEEE Trans. Smart Grid*, vol. 9, no. 4, pp. 2918–2929, Jul. 2018.

[36] S. Chanda and A.K. Srivastava, "Quantifying resiliency of smart power distribution systems with distributed energy resources," in *Proc. IEEE 24th Int. Symp. Ind. Electron.*, 2015, pp. 766–771.

[37] S. Chanda, A. K. Srivastava, M. U. Mohanpurkar, and R. Hovsapian, "Quantifying power distribution system resiliency using code-based metric," *IEEE Trans. Ind. Appl.*, vol. 54, no. 4, pp. 3676–3686, Jul./Aug. 2018.

[38] I. Diahovchenko, G. Kandaperumal, and A. Srivastava, "Distribution power system resiliency improvement using distributed generation and automated switching," in *Proc. IEEE 6th Int. Conf. Energy Smart Syst.*, 2019, pp. 126–131.

[39] S. Pandey, S. Srivastava, G. Kandaperumal, A. K. Srivastava, M. U. Mohanpurkar, and R. Hovsapian, "Optimal operation for resilient and economic modes in an islanded alaskan grid," in *Proc. IEEE Power Energy Soc. Gen. Meeting*, 2020, pp. 1–5.

[40] T. L. Saaty, "Decision making–the analytic hierarchy and network processes (AHP/ANP)," *J. Syst. Sci. Syst. Eng.*, vol. 13, no. 1, pp. 1–35, 2004.

[41] G. Anshuman, J. Kandaperumal, S. L.Pannala, and A. Srivastava, "RT-RMS: A real-time resiliency management system for operational decision support," in *Proc. North Amer. Power Symp.*, 2021, pp. 1–6.

[42] G. Kandaperumal, S. Pandey, and A. Srivastava, "AWR: Anticipate, withstand, and recover resilience metric for operational and planning decision support in electric distribution system," *IEEE Trans. Smart Grid*, vol. 13, no. 1, pp. 179–190, Jan. 2022.